scientific reports

Check for updates

OPEN

On the adsorption characteristics and mechanism of methylene blue by ball mill modified biochar

Jinxia Wang[1,4]✉, Yunfeng Tan[2,4], Hongjun Yang[3]✉, Lingling Zhan[1], Guowen Sun[1] & Le Luo[1]

In this study, modified biochar (BRB) was prepared from rice straw by ball milling technique and used for the adsorption of methylene blue (MB) in wastewater. The BRB was characterized by SEM, FTIR and XPS, and the adsorption model and Box–Behnken design were used to optimize the five influencing factors. The results showed that the ball milling technique could increase the content of functional groups (–OH, C=C and C–O, etc.) and aromatic structures on the surface of biochar, thus facilitating the removal of MB. The isotherm model was consistent with the Langmuir adsorption model ($R^2 = 0.947$) and the maximum adsorption capacity was 50.27 mg/g. The adsorption kinetics was consistent with the pseudo-second-order kinetic model ($R^2 = 1$) and the adsorption rate was mainly controlled by chemisorption. The thermodynamic model confirmed that the adsorption process was a spontaneous heat absorption reaction. The maximum adsorption efficiency was 99.78% under the optimal conditions (40℃, pH 8, reaction time = 90 min, dosing amount = 0.1 mg), and the adsorption efficiency could be improved by increasing the pH and BRB dosing amount. The surface functional groups and crystal structure properties of BRB were the main determinants of adsorption, and it was clarified that physical adsorption, electrostatic attraction and π-π interaction were the main mechanisms for the adsorption of MB by BRB. The main mechanisms were clarified. Therefore, BRB is an economic, efficient and green adsorption material with good potential for the removal of dye pollutants in the aqueous environment.

Dyes are colored aromatic organic compounds that absorb light and give color to the visible area. It is widely used in textile, food, rubber, printing, cosmetics, pharmaceutical, plastic, concrete and paper industries[1,2]. The textile industry is the first application field that generates a significant amount of wastewater from dyeing[3]. If wastewater is discharged directly, the dyes in the wastewater can interfere with the growth of aquatic plants by enhancing the absorption of sunlight, thereby reducing their photosynthetic activity and causing serious ecological problems in the environment[4,5]. The most commonly used MB dye is a cationic heterocyclic compound with a chemical formula of $C_{16}H_{18}N_3SCl$[6,7]. It was first synthesized in 1876 by Badische Anilin and Soda Fabrik's Heinrich Caro as an aniline-based synthetic dye and is widely used in the dyeing process of the textile industry. According to research findings, it has been shown that under certain conditions, MB can decompose and produce harmful gases such as carbon monoxide, carbon dioxide, nitrogen oxides, sulfur oxides, and so on. Long-term exposure to MB can cause methemoglobinemia, diarrhea, allergic dermatitis and cancer[8]. Therefore, people have done a lot of research on the removal of MB in wastewater[6,9,10]. The primary methods for removing dyes from wastewater include photocatalytic degradation, ion exchange, adsorption, coagulation, oxidation, and biological treatment[11]. However, adsorption is considered to be one of the most sustainable methods for dye removal because of its simple design, economic feasibility, high efficiency and its environmental friendliness[12–14].

Biochar (BC) is a carbon-rich solid product obtained by biomass pyrolysis under anoxic or anaerobic conditions[15]. In recent years, it has been widely used as an adsorbent in wastewater treatment and soil remediation[16,17]. The raw materials of BC mainly come from agricultural and forestry waste, industrial waste and animal manure[18]. The physical and chemical properties of BC are mainly affected by the source of raw materials[19]. Among them, lignin and cellulose extracted from agricultural and forestry waste can form porous structure, which is conducive to the removal of pollutants through pore filling effect[20]. However, the widespread cultivation of rice means that its straw is not only a rich biomass raw material, but also contains high silica, which

[1]College of Resources and Safety, Chongqing Vocational Institute of Engineering, Chongqing 402260, China. [2]College of River and Ocean Engineering, Chongqing Jiaotong University, Chongqing 400074, China. [3]College of Resources and Environment, Southwest University, Beibei, Chongqing 400715, China. [4]These authors contributed equally: Jinxia Wang and Yunfeng Tan. ✉email: jinxiawang@cqvie.edu.cn; meilirensheng@swu.edu.cn

provides structural advantages in the preparation of BC[21]. Nevertheless, the original BC still has some limitations in adsorbing dye pollutants[22]. In order to overcome this deficiency, the method of surface modification has gradually become a hot topic for researchers in recent years, and a large number of physical and chemical modification technologies have emerged[23]. Among them, ball milling modification is a method of mechanical ball milling of biochar materials, which changes the structure of adsorption materials by reducing the particle size of BC particles, thereby improving the overall performance of biochar[24,25]. Xiang, W et al.[26] prepared hickory wood biochar to adsorb acetone by ball milling technology. The adsorption efficiency was 13.0 times higher than that before ball milling, and the maximum adsorption capacity of acetone reached 103.4 mg/g. Panahi, The research conducted by Amusat et al.[27] demonstrates that ball milling modification technique can enhance the specific surface area, porosity, and pore distribution of wheat straw biochar. It can even influence the structural changes of functional groups. However, there are relatively few studies on MB adsorption by ball milling modified biochar, and the adsorption mechanism is not yet clear.

Therefore, in this paper, rice straw was used as raw material to prepare biochar (RB), and rice ball milling biochar (BRB) was obtained by ball milling modification and used for MB adsorption research. The impact of key parameters (initial methylene blue concentration, BRB dosage, and pH) and their interaction on the removal efficiency of methylene blue was analyzed using response surface methodology. The samples were characterized by scanning electron microscopy (SEM), energy dispersive X-ray analysis (EDX), Fourier transform infrared spectroscopy (FTIR), X-ray diffraction (XRD) and X-ray photoelectron spectroscopy (XPS). The adsorption mechanism of BRB was discussed by combining adsorption kinetics, adsorption thermodynamics and adsorption isotherm model.

Materials and methods

Biochar preparation and reagents

Rice straw was taken from Chongqing, China, and passed through a 20-mesh sieve after being crushed. It was placed in a tube furnace (OTF-1200X, Shenzhen Kejing Zhida Technology Co., Ltd., China). Before the start of pyrolysis, N_2 (100 mL/min) was introduced for 30 min to eliminate residual air. Continuous introduction of N_2 for 2 h at a heating rate of 10 °C/min was conducted at a temperature of 500 °C. After cooling to room temperature, RB was obtained by washing three times with ultrapure water and drying in an oven at 80 °C for 12 h. RB was milled with a planetary ball mill (MITR-YXQM-2L, Changsha Miqi Instruments Co., Ltd., China) for 30 min (1500 rpm) and passed through a 100-mesh sieve to obtain BRB, which was sealed in a glass bottle for subsequent research.

The test water was ultrapure water (18.2 MΩ·cm) (Labonova Direct Pro, Think-lab, Germany). The chemicals used in this study were all analytically pure. Methylene blue ($C_{18}H_{18}ClN_3·3H_2O$) was purchased from Guoyao Group Chemical Reagents Co., Ltd., hydrochloric acid (HCl) was purchased from Chengdu Cologne Chemical Co., Ltd., and sodium hydroxide (NaOH) was purchased from Chongqing Wansheng Chuandong Chemical Co., Ltd. HCl and NaOH were configured with ultrapure water into a 0.5 mol/L solution for solution pH adjustment.

Characterize

The adsorption capacity of adsorbents was primarily influenced by the microstructure of the material, composition of elements, and composition of functional groups. In order to study the structural changes of BRB before and after adsorption, scanning electron microscope (SEM) and X-ray energy dispersive spectrometer (EDS) (ZEISS Gemini 300, OXFORD Xplore, Germany) were used to analyze the morphological characteristics and element types of the samples. At the same time, the functional groups of the samples were analyzed by Fourier transform infrared spectroscopy (FTIR) (Nicolet iS50, Semirfei, USA). The lattice characteristics of the samples were analyzed by X-ray diffractometer (XRD) (Ultma IV, Rigaku, Japan). Cu-Kα was used as the emission source during the test. The tube voltage and tube current were 40 kV and 30 mA, respectively. The scanning angle was 10°–80°, the step size was 0.02°, and the scanning speed was 5°/min. The valence state of the sample elements was analyzed by X-ray photoelectron spectroscopy (XPS) (K-Alpha, Thermo Scientific, USA).

Experimental design and parameter optimization

The adsorption capacity of adsorbents was primarily influenced by the microstructure of the material. In this study, we used a Box–Behnken composite design model to investigate the effects of MB initial concentration, activated carbon dosage, adsorption time, reaction temperature, and pH as experimental parameters, with adsorption efficiency as the response variable. We also examined the impact of elemental composition and functional group composition. The parameters were optimized to obtain the maximum response value. A 5-factor 3-level design (as shown in Table 1) was used, and the number of trials was n = 45. The equation formula for predicting the response value Y was shown in Eq. (1). The software Design-Expert 13.0.1.0 (Stat-Ease Inc, 2021, USA) was used to analyze the variance of the obtained model to determine the significance of the model and regression coefficients[28].

$$Y = \beta_0 + \sum_{i=1}^{k}\beta_i X_i + \sum_{i=1}^{k}\sum_{j=i+1}^{k}\beta_{ij}X_iX_j + \sum_{i=1}^{k}\beta_{ii}X_i^2 + \varepsilon \tag{1}$$

where Y is the dependent variable, X_i, X_j are the coded values of independent variables (i, j = 1, 2, 3, 4, 5), β_0 is a constant; β_i are linear coefficients; β_{ii}, β_{ij} are interaction coefficients; k is the number of input variables (5).

Variables	Unit	Symbol	Variables level		
			Low −1	Center 0	High +1
MB initial concentration	mg/L	X_1	50	100	150
BRB addition amount	G	X_2	0.05	0.1	0.15
Reaction time	min	X_3	30	90	150
Reaction temperature	°C	X_4	20	30	40
pH	–	X_5	6	8	10

Table 1. Factors and levels of response surface analysis.

Adsorption model

Based on the results of the experimental design and parameter optimization section, the following experiments are carried out under the optimal parameter conditions:

Adsorption kinetic model: in order to understand the mechanism of adsorption process, pseudo-first-order kinetics, pseudo-second-order kinetics and intraparticle diffusion model were used to fit the data, and the adsorption kinetic parameters were evaluated. The kinetic model formulas are shown in Eqs. (2), (3) and (4) [29].

$$\text{Pseudo-first-order}: \quad q_t = q_e\left(1 - e^{-k_1 t}\right) \tag{2}$$

$$\text{Pseudo-second-order}: \quad q_t = \frac{k_2 q_e^2 t}{1 + k_2 q_e t} \tag{3}$$

$$\text{Intraparticle diffusion}: \quad q_t = k_P t^{1/2} + C \tag{4}$$

Adsorption isotherm model: in order to study the effect of initial concentration of MB on adsorption behavior, Langmuir and Freundlich models were used for fitting. The adsorption isotherm model was shown in Eqs. (5) and (6) [29].

$$\text{Langmuir}: q_e = \frac{q_m K_L C}{1 + K_L C} \tag{5}$$

$$\text{Freundlich}: q_e = K_F C_e^{1/n} \tag{6}$$

Adsorption thermodynamic model: in order to study the effect of temperature change on adsorption behavior, the adsorption thermodynamic model was used for fitting. The model equations are shown in Eqs. (7) and (8) [29].

$$ln K_d = \frac{\Delta S^0}{R} - \frac{\Delta H^0}{RT} \tag{7}$$

$$\Delta G^0 = -RT ln K_d = \Delta H^0 - T\Delta S^0 \tag{8}$$

In the equation : q_t refers to the adsorption capacity (mg/g) at t (min); q_e is the equilibrium adsorption capacity (mg/g); k_1 is the rate constant of pseudo-first-order kinetic equation (mg/g·min); k_2 is the rate constant of pseudo-second-order kinetic equation (g/mg·min), and k_P is the rate constant of interparticle diffusion model (mg/g·min$^{1/2}$); C is a constant related to the interface thickness. q_m is the maximum adsorption capacity (mg/g); K_L is the Langmuir model adsorption constant (L/mg); K_F is Freundlich model adsorption constant (mg/g(L/mg)$^{1/n}$); n is a non-uniform factor, which is related to the adsorption strength. R is the ideal gas constant, 8.314 J/mol·k; T is the thermodynamic temperature (K) ; K_d is the adsorption equilibrium coefficient; ΔG is the free energy change of adsorption (KJ/mol); ΔH is the standard adsorption heat (KJ/mol); ΔS is the standard entropy change of adsorption (KJ/K).

Testing method

Tests were performed according to 2.3 and 2.4. All experiments were carried out in a 100 mL conical flask to prepare the required concentration of 50 mL MB solution, adjust the pH, and then add a certain dose of BRB, placed in a constant temperature water bath oscillator (150 rpm) for reaction, through 0.45 μm filter membrane, the concentration of MB was determined. All experiments were set up in 3 parallel groups, and the average value was used for data analysis. Finally, the adsorption capacity q_e and removal rate η (%) are calculated at equilibrium, and the calculation equations were shown in Eqs. (9) and (10).

$$q_e = \frac{(C_0 - C_e)V}{m} \tag{9}$$

$$\eta(\%) = \frac{(C_0 - C_e)}{C_0} \times 100\% \tag{10}$$

Where, q_e (mg/L) is the adsorption capacity at equilibrium, η (%) is the removal, C_0 (mg/L) and C_e (mg/L) are the initial and equilibrium concentrations of MB, and m (g) and V (L) are the mass of BRB and the volume of MB solution, respectively.

Study on regeneration

In order to evaluate the reusability of BRB as adsorbent, 0.5 g of MB adsorbed BRB was added to 50 mL of 0.1 mol/L NaOH solution, and then regenerated by continuous magnetic stirring for 45 min at room temperature. The regenerated BRB was washed three times with ultrapure water to effectively remove the desorbed MB. The regenerated BRB was repeated for 5 adsorption cycles to determine its effectiveness and stability.

Statement stating

For the collection, treatment and all experimental research process of rice straw materials, all comply with the relevant institutions, national and international guidelines and legislation, all procedures were conducted in accordance with the guidelines, and for the rice straw collected in the experiment, we have obtained permission too, hereby declared.

## Results and analysis
Characterize

The surface morphology of BRB before and after adsorption was analyzed by SEM. As shown in Fig. 1, the surface morphology of BRB after adsorption was significantly different compared to that before adsorption. Before adsorption BRB had a relatively smooth surface (Fig. 1a, b), while after adsorption BRB had a rough structure (Fig. 1c, d) with a large number of uniformly dispersed microsphere particle aggregates on its surface, indicating that MB was effectively adsorbed by BRB. The EDX spectra before and after adsorption are presented in Fig. 2 and Fig. S1 (see Supporting Materials). EDX elemental analysis confirmed that the main elements of the biochar were C and O, in addition to Si, K, Ca and Mg, all of which changed significantly before and after adsorption, with the most significant change in Si, whose mass fraction decreased from 14.9 to 4.51%, and related studies indicated that these Mineral components were usually present in biochar in the form of carbonates, phosphates and oxides and may influence the sorption potential of significant biochar related[30]. In addition, the presence of elemental N was not detected in the BRB before adsorption, but after adsorption the mass fraction of elemental N in the BRB increased to 4.57%, which further suggests that the adsorption of MB by BRB was significant.

The functional groups in RB, BRB and BRB after adsorption were analyzed by FTIR, as shown in Fig. 3a. The vibration intensity of the characteristic peaks in the three materials was quite different, and a new characteristic
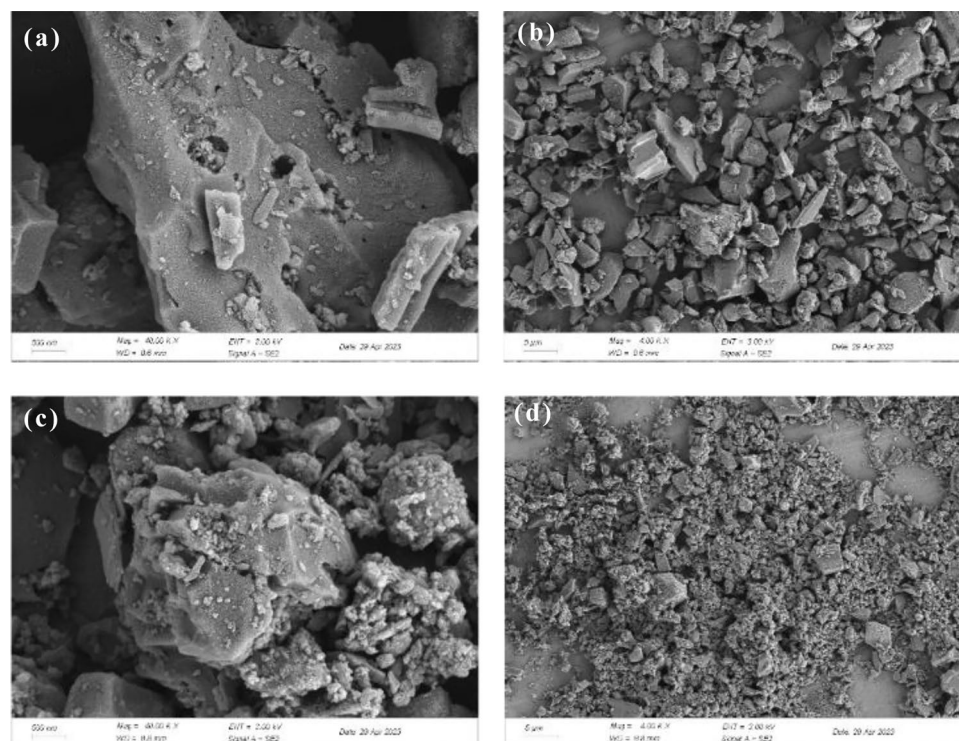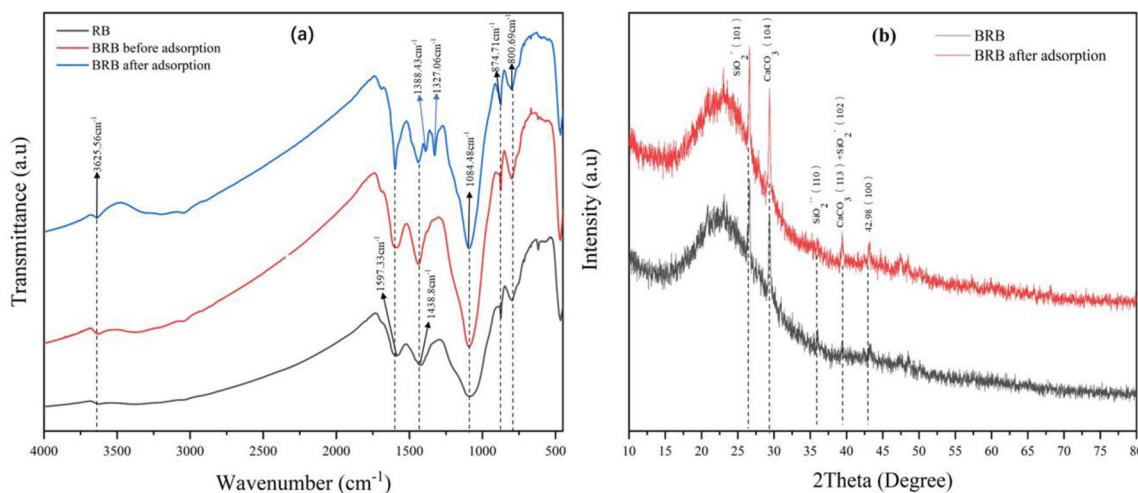

Figure 1. SEM images of PSB [(**a,b**) before adsorption, (**c,d**) after adsorption, at ×40k and ×4k magnification).
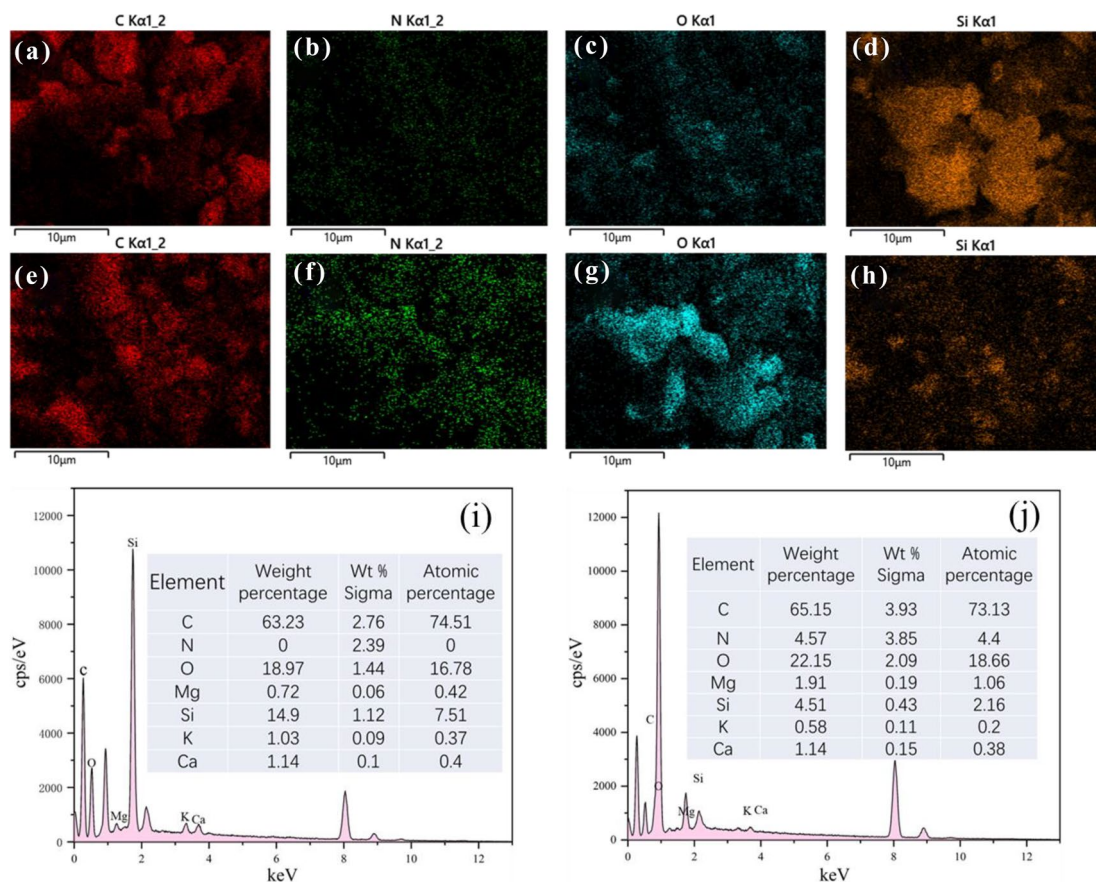
Figure 2. EDX spectra of BRB. (**a–d**), (**i**) BRB before adsorption; (**e–h**), (**j**) BRB after adsorption.


Figure 3. FTIR and XRD of BRB.

peak appears in the adsorbed BRB. For RB, the vibration shrinkage of the characteristic peaks of BRB was significantly stronger than that of RB, and after adsorption of MB, the vibration shrinkage of these characteristic peaks becomes significantly weaker. The changes of characteristic peaks at 3625, 1597, 1438, 1084 and 800 cm^{-1} were mainly attributed to the stretching vibration peaks of –OH group, C=C skeleton in aromatic ring, C–H, C–O and aromatic structure[31–35]. However, new characteristic peaks appeared at 1388 and 1327 cm^{-1}, which were attributed to the methyl and aromatic nitro groups of MB[36,37], indicating that MB interacted significantly with BRB functional groups, which was consistent with the Lyu, HH et al.[38] study. The results show that the material treated by ball milling was more conducive to the removal of MB.

The crystal structure of BRB before and after adsorption was analyzed by XRD. As shown in Fig. 3b, there were characteristic diffraction peaks at 22.62, 26.62, 29.34, 26.04, 29.46, 43.18 and 48.46°. The diffraction peak

at 43.18 (100) indicates the presence of aromatic carbon in BRB and the formation of turbine layer crystallites[39]. Additionally, the presence of calcite ($CaCO_3$) and quartz (SiO_2) microcrystalline phases can be observed in the BRB. The formation of $CaCO_3$ may be related to the high content of calcium oxalate (CaC_2O_4) present in straw[40]. Studies have shown that $CaCO_3$ crystals in biochar from many agricultural and forestry wastes (straw, leaves and wood, etc.) were attributed to the formation of calcite during pyrolysis, and the formation of calcite is beneficial to the increase of alkalinity during the preparation of BRB, thus contributing to its removal of MB[41–43]. The formation of calcite was advantageous in increasing the alkalinity during the preparation process of BRB, thereby facilitating the removal of MB.

The XPS results before and after MB removal by BRB are shown in Fig. 4. Figure 4a mainly presents three significant peaks caused by carbon (C1 s), nitrogen (N1 s) and oxygen (O1 s). The C1 s spectrum at 284.8, 286.8 and 289.4 eV were divided into three peaks (Fig. 5b), which are attributed to the C–C bond, C–O–C bond and O–C=O bond in aliphatic and aromatic compounds, respectively. After adsorption of MB, the percentage of C–C bond decreased from 66.19% before adsorption to 57.49% after adsorption. In addition, the percentages of C–O–C and O–C=O groups increased from 35.32 to 3.49% to 38.68% and 3.82%, respectively, which was mainly attributed to surface complexation and π–π interaction[44,45]. The binding energies of N1s at 399.7 and 402.1 eV were attributed to N in $NSiO_2$ and C–NH_2 bonds, respectively (Fig. 5c). After adsorption, the percentage of $NSiO_2$ bond decreased from 77.29 to 58.79%, which was consistent with the change trend of Si in EDX, indicating that N in MB did not form chemical bonds with Si directly during the adsorption process, but formed n–π interaction with it[46,47]. The percentage of C–NH_2 bond has increased from 22.71 to 44.21%, which was consistent with the observed change in N based on the EDX analysis results. This can be attributed to the formation of aromatic nitro groups during the adsorption process, which is consistent with the results of FTIR analysis. The successful adsorption of MB has been further confirmed. The binding energies of O1 s at 532.9 and 531.2 eV were attributed to O in C=O bond and C–O bond (Fig. 5d). After the adsorption reaction, the percentage of C=O bond decreased from 76.35 to 72.25%, and the percentage of C–O bond increased from 23.65 to 27.75%. This may be due to the fact that some M–O bonds in the metal oxides of BRB in biochar are converted into M–OH, which leads to an increase in hydroxyl functional groups, and also indicates that oxygen-containing functional groups play an important role in removing MB.
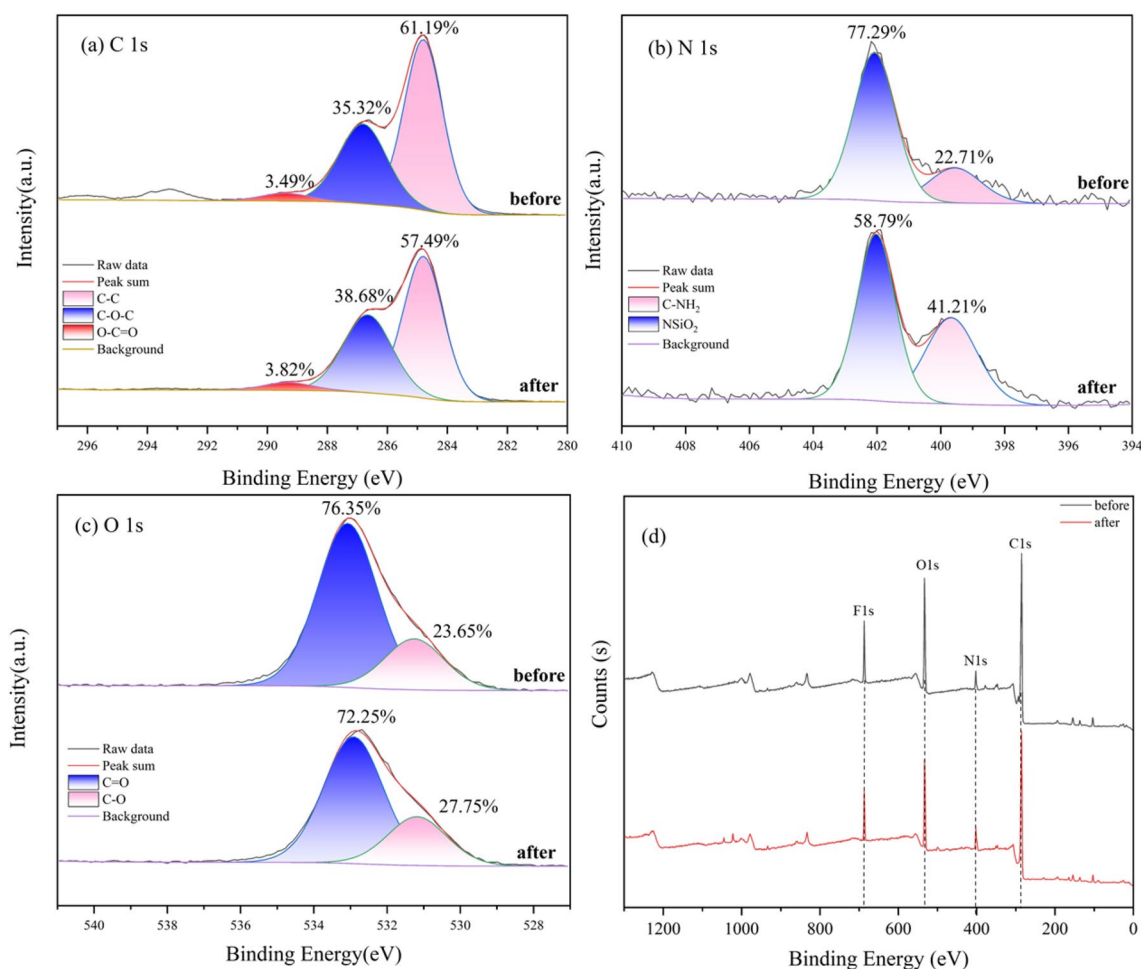
Figure 4. XPS of BRB before and after MB adsorption.
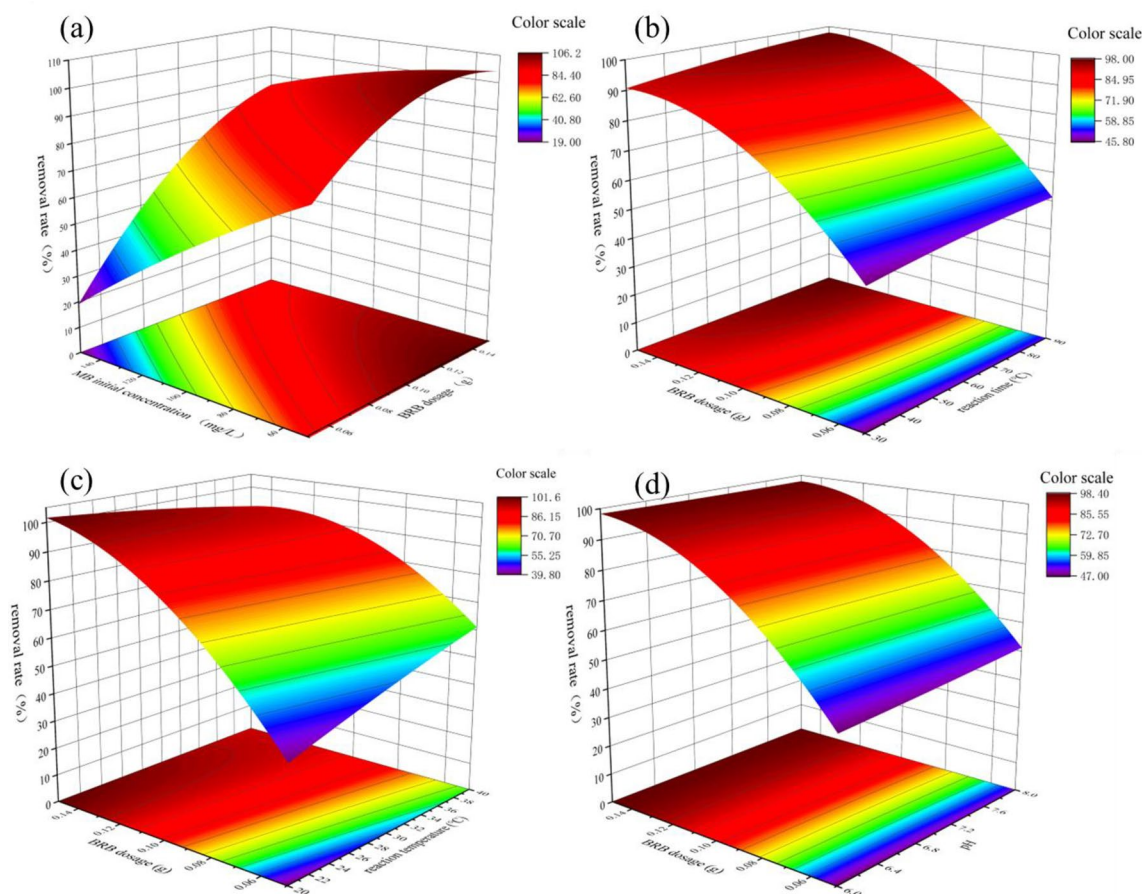
Figure 5. 3D response surface (**a**) effect of initial MB concentration and BRB dosage; (**b**) effects of BRB dosage and reaction time; (**c**) the effects of BRB dosage and reaction temperature; (**d**) the 3D diagram of the effects of BRB dosage and pH.

Experimental design and parameter optimization

The experimental results based on RSM are shown in Table S1. The fitted quadratic polynomial equation was given in Eq. (11):

$$
\begin{aligned}
Y = {}& 85.21 - 19.24 \times X_1 + 23.27 \times X_2 + 2.34 \times X_3 + 2.53 \times X_4 + 2.64 \times X_5 + 10.07 \times X_1 \times X_2 \\
& + 1.83 \times X_1 \times X_3 + 0.9415 \times X_1 \times X_4 + 2.59 \times X_1 \times X_5 + 0.9379 \times X_2 \times X_3 - 7.57 \times X_2 \times X_4 \\
& - 2.39 \times X_2 \times X_5 + 1.2 \times X_3 \times X_4 + 0.1617 \times X_3 \times X_5 - 0.1617 \times X_4 \times X_5 - 2.81 \times X_1^2 \\
& - 11.36 \times X_2^2 - 3.88 \times X_3^2 - 0.8805 \times X_4^2 + 0.7893 \times X_5^2
\end{aligned}
$$

$$(11)$$

Analysis of variance (ANOVA) (Table S2) was used to determine the statistical significance of all analyses. The statistical significance of the quadratic fit was determined by the LOF, R^2 and R^2_{adj} between the predicted and experimental values. The $p < 0.0001$ indicates that the fitted model is an effective model for predicting experimental values. X_1, X_2, X_5, $X_1 X_2$, $X_2 X_4$ and X_2^2 were statistically significant ($p < 0.05$). Other model terms with $p > 0.05$ were omitted in the model equation to obtain the best fit for the model. $A_{deq} = 24.65$ (precision > 4), so there was a good correlation between the experimental and predicted response[48].

The interaction between variables was studied by 3D response surface. Figure 5a shows that by increasing the amount of BRB from 0.05 to 0.15 g, the removal rate increased from 29.90 to 99.65% with the decrease of MB initial concentration. This can be attributed to an increase in the number of adsorption sites of MB as the dosage increases[49]. Figure 5b shows that by increasing the reaction time from 30 to 90 min, the MB removal rate increases significantly, which may be that MB needs enough time to diffuse more fully inside the BRB[50]. From Fig. 5c, it can be observed that as the temperature increases from 20 to 40 ℃, the removal efficiency of MB increases from 56.18 to 86.71%. This indicates that temperature has a significant impact on the removal of MB. Figure 5d shows that pH has a significant effect on MB removal rate. When the pH value was greater than the zero point of BRB (pH_{zpc}), the BRB surface will obtain negative charge and promote the adsorption of MB by electrostatic attraction[51], as described in the following equation.

$$
BRB - O^- + MB^+ \leftrightarrow BRB - O^- \cdots\cdots {}^+MB
$$

$$(12)$$
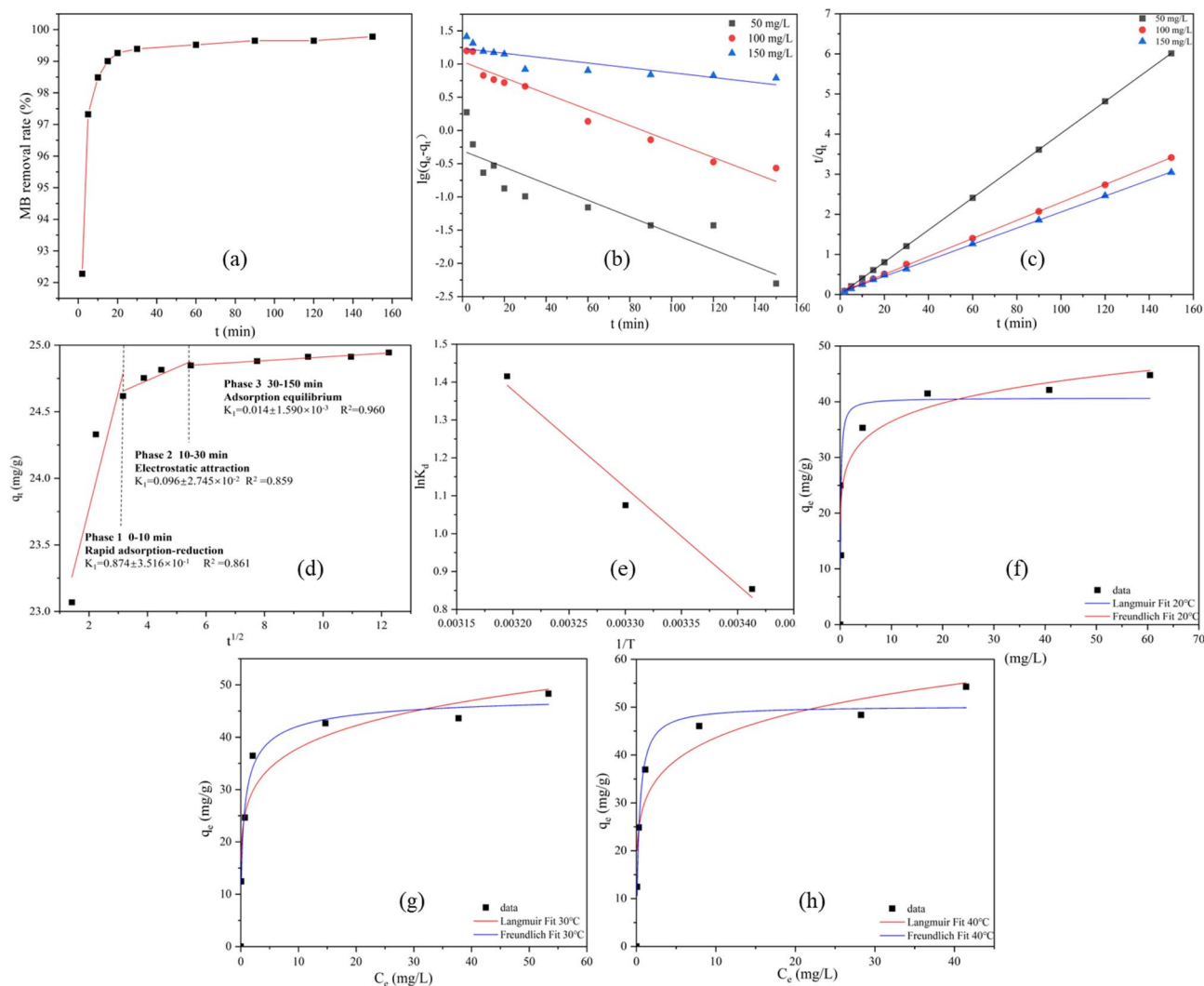
Figure 6. MB adsorption model of BRB: (**a**) t-adsorption rate curve; (**b–d**) pseudo-first-order, pseudo-second-order dynamic model and particle diffusion model; (**e**) thermodynamic model; (**f–h**) isotherm model (BRB dosage = 0.1 g, MB initial concentration = 100 mg/g; temperature = 20, 30 and 40 °C; pH 7, reaction time = 180 min).

Model investigation

The experimental data were simulated by kinetic models (pseudo-first-order, pseudo-second-order and inter-particle), and the adsorption process of MB on BRB was analyzed. The simulation results for the adsorption of MB on BRB using three different kinetic models are shown in Fig. 6. Figure 6a illustrates the effect of contact time on the removal of MB from BRB, indicating that the initial 20 min constitute a rapid adsorption phase followed by an adsorption equilibrium phase. And when the adsorption equilibrium was reached, it tends to be stable immediately. This rapid adsorption was due to the fact that BRB provides relatively more adsorption sites at the initial stage of adsorption. Using the pseudo-first-order and pseudo-second-order models (Fig. 6a, b). When the initial concentration of MB was 50, 100 and 150 mg/L, R^2 reaches 1, 0.9998 and 0.9997, respectively, while the pseudo-first-order model was 0.7434, 0.9508 and 0.8285 (Tables S3, S4). The pseudo-second-order model was superior to the pseudo-first-order model. This was because chemical adsorption controls the rate of the adsorption process[52].

The adsorption behavior was mainly manifested as surface adsorption and pore adsorption. In order to comprehend the adsorption behavior of BRB, a particle internal diffusion model was employed. As shown in Fig. 6d, the adsorption process was divided into three stages. Among them, the value of K was not zero, and the curve does not pass the origin, so the mechanism was not the only limiting process. The adsorption of MB on BRB was a complex multi-factor control process[53–55]. In the first stage of adsorption, the K_1 value was high (K_1 = 0.874), indicating that the adsorption of MB mainly occurs on the BRB surface and diffuses faster. In the second stage, as the adsorption sites on the surface of BRB are gradually occupied, MB gradually diffuses into the internal pores of biochar. Since the K_2 value (K_2 = 0.096) was significantly lower than that in the first stage, the adsorption efficiency was limited by the intraparticle diffusion, resulting in the internal diffusion efficiency

lower than the surface diffusion[56,57]. In the third stage, the K_3 value decreased to a lower value ($K_3 = 0.014$), which was a slow intraparticle diffusion process due to the occupation of intraparticle space.

The temperature has a significant effect on the removal effect. Figure 6e and Fig. S5 were the thermodynamic models and parameters of MB adsorption by BRB. When the ($\Delta G°$) value was less than zero (-2.08, -2.71 and -3.68), the adsorption rate of MB by BRB increases with the increase of temperature, indicating that this was a spontaneous adsorption process[58]. When $\Delta H°$ was greater than zero (21.35 kJ/mol), the adsorption process was an endothermic reaction. $\Delta S°$ was greater than zero (79.79 kJ/mol), indicating the affinity of BRB to MB. Therefore, the adsorption of MB on BRB was an endothermic reaction of spontaneous adsorption.

In addition, the Langmuir and Freundlich isothermal models (Fig. 6f–h) were analyzed. The fitting parameters are shown in Fig. S6.

As the temperature increases, the Langmuir model ($R_2 = 0.974$) outperforms the Freundlich model ($R_2 = 0.898$), indicating a greater tendency for dye adsorption to occur through a monolayer process[59]. The adsorption capacity increased with the increase of temperature, and the maximum adsorption capacity of Langmuir was 50.270 mg/g at 40 ℃.

Regeneration research

The regeneration capacity of adsorbents was considered to be a major parameter for economic and environmental applications. The results of the adsorption–desorption cycle of BRB shown in Fig. S2 show that the regenerated adsorbent can be reused for at least four adsorption–desorption cycles without changing its effectiveness. However, the observed decrease in adsorption efficiency after the third cycle can be attributed to the deposition of MB molecules on the surface of the BRB during the regeneration process.

Adsorption mechanism

Figure 7 was the adsorption mechanism diagram of BRB on MB, which mainly includes the following mechanisms: (1) Physical adsorption.

The analysis of the SEM image in Fig. 1 reveals the presence of deposits on the surface of the biochar. This suggests that the Binding Reagent BRB effectively removes the MB by undergoing surface adsorption and pore filling, leading to the formation of these deposits[22]. Based on the results of the intraparticle diffusion model, it was shown that among them physical adsorption was the main mechanism for MB removal; (2) the infrared results confirmed the existence of –OH and C=O functional groups in BRB, which could promote the complexation of positively charged MB dye molecules with the surface active groups of BRB[60,61]; (3) when $pH > pH_{zpc}$, the surface functional groups (–OH, –COOH and –NH$_3$, etc.) of BRB are deprotonated, and BRB has a good electrostatic attraction to MB. When $pH < pH_{zpc}$, the surface of BRB was protonated, and the adsorption effect of MB cations was significantly reduced due to electrostatic repulsion[62,63]. The response surface analysis results indicate that BRB exhibits the highest adsorption performance at pH 8; (4) The π–π interaction occurs between the π–electron system of the BRB structure and the aromatic group of the MB dye molecule[64]; (5) the presence of Si–O–Si groups was confirmed by n–π interaction, EDX and XPS results, and the presence of Si–O–Si in alkaline solution was beneficial to the adsorption of MB, thus revealing the n–π interaction between the aromatic structure of MB and the Si–O–Si of BRB[65,66]; (6) in other reactions, the hydrogen bonds
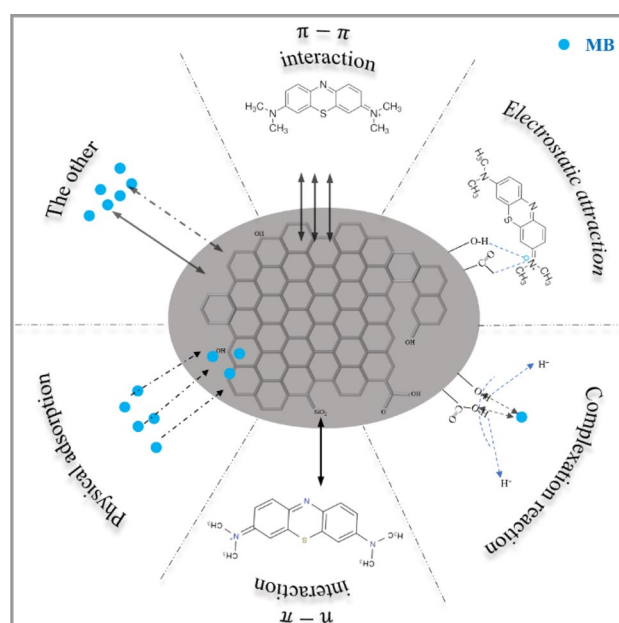
Figure 7. Mechanism diagram of BRB adsorbing MB.

formed between the free H$^+$ on the BRB surface and the O and N in MB are predominantly non-electrostatic, potentially serving as an adsorption mechanism in the reaction system[67,68]. On the other hand, EDX results showed that the contents of various inorganic minerals (Ca^{2+}, Mg^{2+} and K$^+$, etc.) changed significantly before and after the adsorption of BRB, indicating that these minerals were released from the surface of biochar during the adsorption of MB, allowing ion exchange to occur[69].

Conclusions

BRB was prepared using a ball milling technique and the adsorption behavior and mechanism of BRB on MB was analyzed. The successful adsorption of MB on the surface of BRB was confirmed by various characterization techniques. The adsorption kinetic study showed that the adsorption behavior of MB followed pseudo-second order kinetics ($R^2 = 1$) and Langmuir isotherm adsorption model ($R^2 = 0.947$), and chemisorption was the decisive step for adsorption efficiency with the maximum adsorption capacity of 50.27 mg/g. Thermodynamic analysis showed that the adsorption process of BRB on MB was a spontaneous heat absorption process. The maximum adsorption efficiency reached 99.78% under the optimal conditions (temperature = 40℃, pH 8, reaction time = 90 min, and dosing amount of 0.1 mg). In summary, physical adsorption, electrostatic attraction and π–π interaction may be the main mechanisms for the adsorption of MB by BRB. Therefore, it provides a simple and cost-effective way to achieve recycling of agricultural waste and water purification of organic pollutants.

Data availability

The data used to support the findings of this study are available from the corresponding author upon request.

References

1. Khan, I. *et al.* Review on methylene blue: Its properties, uses, toxicity and photodegradation. *Water* https://doi.org/10.3390/w14020242 (2022).
2. Kumar, P. S. *et al.* A critical review on recent developments in the low-cost adsorption of dyes from wastewater. *Desalin. Water Treat.* **172**, 395–416. https://doi.org/10.5004/dwt.2019.24613 (2019).
3. Ben Slama, H. *et al.* Diversity of synthetic dyes from textile industries, discharge impacts and treatment methods. *Appl. Sci.-Basel* https://doi.org/10.3390/app11146255 (2021).
4. Al-Tohamy, R. *et al.* A critical review on the treatment of dye-containing wastewater: Ecotoxicological and health concerns of textile dyes and possible remediation approaches for environmental safety. *Ecotoxicol. Environ. Saf.* https://doi.org/10.1016/j.ecoenv.2021.113160 (2022).
5. Sharma, J., Sharma, S. & Soni, V. Classification and impact of synthetic textile dyes on aquatic flora: A review. *Region. Stud. Mar. Sci.* https://doi.org/10.1016/j.rsma.2021.101802 (2021).
6. Mashkoor, F. & Abu, N. Magsorbents: Potential candidates in wastewater treatment technology—A review on the removal of methylene blue dye. *J. Magnet. Magnet. Mater.* https://doi.org/10.1016/j.jmmm.2020.166408 (2020).
7. Arabi, S. & Sohrabi, M. R. Removal of methylene blue, a basic dye, from aqueous solutions using nano-zerovalent iron. *Water Sci. Technol.* **70**, 24–31. https://doi.org/10.2166/wst.2014.189 (2014).
8. Sahu, S. *et al.* Adsorption of methylene blue on chemically modified lychee seed biochar: Dynamic, equilibrium, and thermodynamic study. *J. Mol. Liq.* https://doi.org/10.1016/j.molliq.2020.113743 (2020).
9. Wu, Z. B. *et al.* Adsorptive removal of methylene blue by rhamnolipid-functionalized graphene oxide from wastewater. *Water Res.* **67**, 330–344. https://doi.org/10.1016/j.watres.2014.09.026 (2014).
10. Gupta, R. *et al.* Potential and future prospects of biochar-based materials and their applications in removal of organic contaminants from industrial wastewater. *J. Mater. Cycl. Waste Manag.* **24**, 852–876. https://doi.org/10.1007/s10163-022-01391-z (2022).
11. Ahmad, A. *et al.* Recent advances in new generation dye removal technologies: Novel search for approaches to reprocess wastewater. *Rsc Adv.* **5**, 30801–30818. https://doi.org/10.1039/c4ra16959j (2015).
12. Rashid, R., Shafiq, I., Akhter, P., Iqbal, M. J. & Hussain, M. A state-of-the-art review on wastewater treatment techniques: The effectiveness of adsorption method. *Environ. Sci. Pollut. Res.* **28**, 9050–9066. https://doi.org/10.1007/s11356-021-12395-x (2021).
13. Salman, M. S. *et al.* Chitosan-coated cotton fiber composite for efficient toxic dye encapsulation from aqueous media. *Appl. Surf. Sci.* https://doi.org/10.1016/j.apsusc.2023.157008 (2023).
14. Liu, Y. Y. *et al.* Fabrication of multifunctional biomass-based aerogel with 3D hierarchical porous structure from waste reed for the synergetic adsorption of dyes and heavy metal ions. *Chem. Eng. J.* https://doi.org/10.1016/j.cej.2022.138934 (2023).
15. Pan, X. Q., Gu, Z. P., Chen, W. M. & Li, Q. B. Preparation of biochar and biochar composites and their application in a Fenton-like process for wastewater decontamination: A review. *Sci. Total Environ.* https://doi.org/10.1016/j.scitotenv.2020.142104 (2021).
16. Xiang, W. *et al.* Biochar technology in wastewater treatment: A critical review. *Chemosphere.* https://doi.org/10.1016/j.chemosphere.2020.126539 (2020).
17. Ren, S. X. *et al.* A review on current pollution and removal methods of tetracycline in soil. *Sep. Sci. Technol.* https://doi.org/10.1080/01496395.2023.2259079 (2023).
18. Elkhlifi, Z. *et al.* Potential role of biochar on capturing soil nutrients, carbon sequestration and managing environmental challenges: A review. *Sustainability.* https://doi.org/10.3390/su15032527 (2023).
19. Jiang, H. T. & Dai, Y. J. Vitamin C modified crayfish shells biochar efficiently remove tetracycline from water: A good medicine for water restoration. *Chemosphere.* https://doi.org/10.1016/j.chemosphere.2022.136884 (2023).
20. Zhu, R. *et al.* Analysis of factors influencing pore structure development of agricultural and forestry waste-derived activated carbon for adsorption application in gas and liquid phases: A review. *J. Environ. Chem. Eng.* https://doi.org/10.1016/j.jece.2021.105905 (2021).
21. Singh, R. & Patel, M. Effective utilization of rice straw in value-added by-products: A systematic review of state of art and future perspectives. *Biomass Bioenergy.* https://doi.org/10.1016/j.biombioe.2022.106411 (2022).
22. Liang, L. P. *et al.* Review of organic and inorganic pollutants removal by biochar and biochar-based composites. *Biochar.* **3**, 255–281. https://doi.org/10.1007/s42773-021-00101-6 (2021).
23. Liu, X. *et al.* New use for *Lentinus edodes* bran biochar for tetracycline removal. *Environ. Res.* https://doi.org/10.1016/j.envres.2022.114651 (2023).
24. Kumar, M. *et al.* Ball milling as a mechanochemical technology for fabrication of novel biochar nanomaterials. *Bioresour. Technol.* https://doi.org/10.1016/j.biortech.2020.123613 (2020).

25. Zhuang, Z. C., Wang, L. & Tang, J. C. Efficient removal of volatile organic compound by ball-milled biochars from different preparing conditions. *J. Hazard. Mater.* https://doi.org/10.1016/j.jhazmat.2020.124676 (2021).

26. Xiang, W. *et al.* Enhanced adsorption performance and governing mechanisms of ball-milled biochar for the removal of volatile organic compounds (VOCs). *Chem. Eng. J.* https://doi.org/10.1016/j.cej.2019.123842 (2020).

27. Amusat, S. O., Kebede, T. G., Dube, S. & Nindi, M. M. Ball-milling synthesis of biochar and biochar-based nanocomposites and prospects for removal of emerging contaminants: A review. *J. Water Process Eng.* https://doi.org/10.1016/j.jwpe.2021.101993 (2021).

28. Foroughi, M., Azqhandi, M. H. A. & Kakhki, S. Bio-inspired, high, and fast adsorption of tetracycline from aqueous media using Fe$_3$O$_4$-g-CN@PEI-beta-CD nanocomposite: Modeling by response surface methodology (RSM), boosted regression tree (BRT), and general regression neural network (GRNN). *J. Hazard. Mater.* https://doi.org/10.1016/j.jhazmat.2019.121769 (2020).

29. Yao, X. X. *et al.* Magnetic activated biochar nanocomposites derived from wakame and its application in methylene blue adsorption. *Bioresour. Technol.* https://doi.org/10.1016/j.biortech.2020.122842 (2020).

30. Xu, X. Y. *et al.* Indispensable role of biochar-inherent mineral constituents in its environmental applications: A review. *Bioresour. Technol.* **241**, 887–899. https://doi.org/10.1016/j.biortech.2017.06.023 (2017).

31. Zheng, Y. L., Wan, Y. S., Chen, J. J., Chen, H. & Gao, B. MgO modified biochar produced through ball milling: A dual-functional adsorbent for removal of different contaminants. *Chemosphere.* https://doi.org/10.1016/j.chemosphere.2019.125344 (2020).

32. Chi, T., Zuo, J. & Liu, F. L. Performance and mechanism for cadmium and lead adsorption from water and soil by corn straw biochar. *Front. Environ. Sci. Eng.* https://doi.org/10.1007/s11783-017-0921-y (2017).

33. Zhang, Y. *et al.* Pyrolysis-temperature depended quinone and carbonyl groups as the electron accepting sites in barley grass derived biochar. *Chemosphere.* **232**, 273–280. https://doi.org/10.1016/j.chemosphere.2019.05.225 (2019).

34. Cho, D. W., Yoon, K., Kwon, E. E., Biswas, J. K. & Song, H. Fabrication of magnetic biochar 'as a treatment medium for As(V) via pyrolysis of FeCl$_3$-pretreated spent coffee ground. *Environ. Pollut.* **229**, 942–949. https://doi.org/10.1016/j.envpol.2017.07.079 (2017).

35. Zhao, M., Wang, A. M., Cao, D. Y., Wei, Y. C. & Ding, L. Q. Differences in macromolecular structure evolution during the pyrolysis of vitrinite and inertinite based on in situ FTIR and XRD measurements. *Energies.* https://doi.org/10.3390/en15155334 (2022).

36. Godzierz, M. *et al.* Facile and highly efficient wet synthesis of nanocrystalline BiFeO$_3$ particles by reverse co-precipitation method. *Ceram. Int.* **49**, 12126–12137. https://doi.org/10.1016/j.ceramint.2022.12.064 (2023).

37. Fu, J. Q. *et al.* Study on the evolution pattern of the chemical structure of Fenton pretreated lignin during hydrothermal carbonization. *J. Environ. Chem. Eng.* https://doi.org/10.1016/j.jece.2022.107184 (2022).

38. Lyu, H. H. *et al.* Experimental and modeling investigations of ball-milled biochar for the removal of aqueous methylene blue. *Chem. Eng. J.* **335**, 110–119. https://doi.org/10.1016/j.cej.2017.10.130 (2018).

39. Deshan, A. D. K. *et al.* Transforming cotton gin trash to engineered functional carbon structures. *Adv. Sustain. Syst.* https://doi.org/10.1002/adsu.202100061 (2021).

40. Andriopoulou, N. C. & Christidis, G. E. Multi-analytical characterisation of wheat biominerals: Impact of methods of extraction on the mineralogy and chemistry of phytoliths. *Archaeol. Anthropol. Sci.* https://doi.org/10.1007/s12520-020-01091-5 (2020).

41. Qiu, G. Q. *et al.* Biochar synthesized via pyrolysis of *Broussonetia papyrifera* leaves: Mechanisms and potential applications for phosphate removal. *Environ. Sci. Pollut. Res.* **26**, 6565–6575. https://doi.org/10.1007/s11356-018-04095-w (2019).

42. Ramola, S. *et al.* Preparation and application of novel rice husk biochar–calcite composites for phosphate removal from aqueous medium. *J. Clean. Prod.* https://doi.org/10.1016/j.jclepro.2021.126802 (2021).

43. Saadat, S., Raei, E. & Talebbeydokhti, N. Enhanced removal of phosphate from aqueous solutions using a modified sludge derived biochar: Comparative study of various modifying cations and RSM based optimization of pyrolysis parameters. *J. Environ. Manag.* **225**, 75–83. https://doi.org/10.1016/j.jenvman.2018.07.037 (2018).

44. Chen, X. N., Wang, X. & Fang, D. A review on C1s XPS-spectra for some kinds of carbon materials. *Fullerenes Nanotubes Carbon Nanostruct.* **28**, 1048–1058. https://doi.org/10.1080/1536383x.2020.1794851 (2020).

45. Prarat, P., Hongsawat, P. & Punyapalakul, P. Amino-functionalized mesoporous silica-magnetic graphene oxide nanocomposites as water-dispersible adsorbents for the removal of the oxytetracycline antibiotic from aqueous solutions: Adsorption performance, effects of coexisting ions, and natural organic matter. *Environ. Sci. Pollut. Res.* **27**, 6560–6576. https://doi.org/10.1007/s11356-019-07186-4 (2020).

46. Tran, H. N. *et al.* Innovative spherical biochar for pharmaceutical removal from water: Insight into adsorption mechanism. *J. Hazard. Mater.* https://doi.org/10.1016/j.jhazmat.2020.122255 (2020).

47. Huang, Q. *et al.* Biochar-based materials and their applications in removal of organic contaminants from wastewater: State-of-the-art review. *Biochar.* **1**, 45–73. https://doi.org/10.1007/s42773-019-00006-5 (2019).

48. Ganesan, V. *et al.* Optimisation of mechanical properties in saw-dust/woven-jute fibre/polyester structural composites under liquid nitrogen environment using response surface methodology. *Polymers.* https://doi.org/10.3390/polym13152471 (2021).

49. Ambaye, T. G., Vaccari, M., van Hullebusch, E. D., Amrane, A. & Rtimi, S. Mechanisms and adsorption capacities of biochar for the removal of organic and inorganic pollutants from industrial wastewater. *Int. J. Environ. Sci. Technol.* **18**, 3273–3294. https://doi.org/10.1007/s13762-020-03060-w (2021).

50. Qiu, B. B., Shao, Q. N., Shi, J. C., Yang, C. H. & Chu, H. Q. Application of biochar for the adsorption of organic pollutants from wastewater: Modification strategies, mechanisms and challenges. *Sep. Purif. Technol.* https://doi.org/10.1016/j.seppur.2022.121925 (2022).

51. Ramanayaka, S. *et al.* Performance of metal-organic frameworks for the adsorptive removal of potentially toxic elements in a water system: A critical review. *Rsc Adv.* **9**, 34359–34376. https://doi.org/10.1039/c9ra06879a (2019).

52. El Maguana, Y., Elhadiri, N., Benchanaa, M. & Chikri, R. Activated carbon for dyes removal: Modeling and understanding the adsorption process. *J. Chem.* https://doi.org/10.1155/2020/2096834 (2020).

53. Banerjee, S. & Chattopadhyaya, M. C. Adsorption characteristics for the removal of a toxic dye, tartrazine from aqueous solutions by a low cost agricultural by-product. *Arab. J. Chem.* **10**, S1629–S1638. https://doi.org/10.1016/j.arabjc.2013.06.005 (2017).

54. Marzbali, M. H., Mir, A. A., Pazoki, M., Pourjamshidian, R. & Tabeshnia, M. Removal of direct yellow 12 from aqueous solution by adsorption onto spirulina algae as a high-efficiency adsorbent. *J. Environ. Chem. Eng.* **5**, 1946–1956. https://doi.org/10.1016/j.jece.2017.03.018 (2017).

55. Andrade, C. A. *et al.* Adsorption behavior and mechanism of oxytetracycline on rice husk ash: Kinetics, equilibrium, and thermodynamics of the process. *Water Air Soil Pollut.* https://doi.org/10.1007/s11270-020-04473-6 (2020).

56. Lin, D. Y. *et al.* Adsorption of dye by waste black tea powder: Parameters, kinetic, equilibrium, and thermodynamic studies. *J. Chem.* https://doi.org/10.1155/2020/5431046 (2020).

57. Liu, H. B., Shan, J. H., Chen, Z. B. & Lichtfouse, E. Efficient recovery of phosphate from simulated urine by Mg/Fe bimetallic oxide modified biochar as a potential resource. *Sci. Total Environ.* https://doi.org/10.1016/j.scitotenv.2021.147546 (2021).

58. Wang, S. A. *et al.* A study on and adsorption mechanism of ammonium nitrogen by modified corn straw biochar. *R. Soc. Open Sci.* https://doi.org/10.1098/rsos.221535 (2023).

59. Altun, T. & Ecevit, H. Adsorption of malachite green and methyl violet 2B by halloysite nanotube: Batch adsorption experiments and Box–Behnken experimental design. *Mater. Chem. Phys.* https://doi.org/10.1016/j.matchemphys.2022.126612 (2022).

60. Zare, E. N. *et al.* Smart adsorbents for aquatic environmental remediation. *Small.* https://doi.org/10.1002/smll.202007840 (2021).

61. Darabdhara, J. & Ahmaruzzaman, M. Recent developments in MOF and MOF based composite as potential adsorbents for removal of aqueous environmental contaminants. *Chemosphere.* https://doi.org/10.1016/j.chemosphere.2022.135261 (2022).

62. Shaikh, W. A., Ul Islam, R. & Chakraborty, S. Stable silver nanoparticle doped mesoporous biochar-based nanocomposite for efficient removal of toxic dyes. *J. Environ. Chem. Eng.* https://doi.org/10.1016/j.jece.2020.104982 (2021).

63. Sahnoun, A. Y. *et al.* Valorization of sewage sludge for methylene blue removal from aqueous solution. *Biomass Convers. Biorefin.* https://doi.org/10.1007/s13399-022-03012-z (2022).

64. Wathukarage, A., Herath, I., Iqbal, M. C. M. & Vithanage, M. Mechanistic understanding of crystal violet dye sorption by woody biochar: Implications for wastewater treatment. *Environ. Geochem. Health* **41**, 1647–1661. https://doi.org/10.1007/s10653-017-0013-8 (2019).

65. Al-Ghouti, M. A., Khan, M., Nasser, M. S., Al Saad, K. & Heng, O. Application of geopolymers synthesized from incinerated municipal solid waste ashes for the removal of cationic dye from water. *Plos One.* https://doi.org/10.1371/journal.pone.0239095 (2020).

66. Wang, Y., Zhang, Y., Li, S. Y., Zhong, W. H. & Wei, W. Enhanced methylene blue adsorption onto activated reed-derived biochar by tannic acid. *J. Mol. Liq.* **268**, 658–666. https://doi.org/10.1016/j.molliq.2018.07.085 (2018).

67. Singh, S., Prajapati, A. K., Chakraborty, J. P. & Mondal, M. K. Adsorption potential of biochar obtained from pyrolysis of raw and torrefied *Acacia nilotica* towards removal of methylene blue dye from synthetic wastewater. *Biomass Convers. Biorefin.* https://doi.org/10.1007/s13399-021-01645-0 (2021).

68. Mohan, D., Sarswat, A., Ok, Y. S. & Pittman, C. U. Organic and inorganic contaminants removal from water with biochar, a renewable, low cost and sustainable adsorbent—A critical review. *Bioresour. Technol.* **160**, 191–202. https://doi.org/10.1016/j.biortech.2014.01.120 (2014).

69. Munera-Echeverri, J. L. *et al.* Cation exchange capacity of biochar: An urgent method modification. *Sci. Total Environ.* **642**, 190–197. https://doi.org/10.1016/j.scitotenv.2018.06.017 (2018).

Author contributions

J.W., Experiment, Software, Writing-Original draft preparation; Y.T., Experiment, Data curation, Writing-Original draft preparation; H.Y., Methodology, Investigation, Data curation; L.Z., Data collection, Editing. G.S., L.L., Software analysis, Experimental operation.

Competing interests

The authors declare no competing interests.

Additional information

Supplementary Information The online version contains supplementary material available at https://doi.org/10.1038/s41598-023-48373-1.

Correspondence and requests for materials should be addressed to J.W. or H.Y.

Reprints and permissions information is available at www.nature.com/reprints.

Publisher's note Springer Nature remains neutral with regard to jurisdictional claims in published maps and institutional affiliations.